Neuron
Article

Synaptic Encoding of Fear Extinction in mPFC-amygdala Circuits

Jun-Hyeong Cho,[1] Karl Deisseroth,[2] and Vadim Y. Bolshakov[1,*]
[1]Department of Psychiatry, McLean Hospital, Harvard Medical School, Belmont, MA 02478, USA
[2]Department of Bioengineering, Department of Psychiatry and Behavioral Sciences, Howard Hughes Medical Institute, Stanford University, Stanford, CA 94305, USA
*Correspondence: vadimb@mclean.harvard.edu
http://dx.doi.org/10.1016/j.neuron.2013.09.025

SUMMARY

Retrieval of fear extinction memory is associated with increased firing of neurons in the medial prefrontal cortex (mPFC). It is unknown, however, how extinction learning-induced changes in mPFC activity are relayed to target structures in the amygdala, resulting in diminished fear responses. Here, we show that fear extinction decreases the efficacy of excitatory synaptic transmission in projections from the mPFC to the basolateral nucleus of the amygdala (BLA), whereas inhibitory responses are not altered. In contrast, synaptic strength at direct mPFC inputs to intercalated neurons remains unchanged after extinction. Moreover, priming stimulation of mPFC projections induced heterosynaptic inhibition in auditory cortical inputs to the BLA. These synaptic mechanisms could contribute to the encoding of extinction memory by diminishing the ability of projections from the mPFC to drive BLA activity while retaining the ability of intercalated neurons to inhibit the output nuclei of the amygdala.

INTRODUCTION

During auditory fear conditioning, experimental subjects learn to associate an emotionally neutral conditioned stimulus (CS; audible tone) with an aversive unconditioned stimulus (US, electric footshock) (LeDoux, 2000; Maren and Quirk, 2004). The lateral nucleus of the amygdala (LA) is a site of synaptic plasticity associated with learning of the CS-US association (Quirk et al., 1995; Rogan et al., 1997; Pape and Pare, 2010). Previous studies demonstrated that long-term potentiation (LTP) in auditory CS projections to the LA might provide a cellular substrate of fear learning (McKernan and Shinnick-Gallagher, 1997; Tsvetkov et al., 2002; Cho et al., 2012). Similar to other forms of classical conditioning, conditioned fear could be diminished following training procedures leading to extinction, when the CS is repeatedly presented without the US (Pavlov, 1927; Maren and Quirk, 2004). It appears, however, that fear extinction does not erase a consolidated memory of the CS-US association but rather results from new learning, inhibiting retrieval of conditioned fear memory.

Presently, there is substantial evidence that projections from the medial prefrontal cortex (mPFC) to the amygdala inhibit expression of conditioned fear, suggesting that fear extinction may depend on the increased neuronal activity in the mPFC after extinction training (Milad and Quirk, 2002; Milad et al., 2004; Santini et al., 2004; Holmes et al., 2012). Consistent with the role of the mPFC in long-term extinction memory, rats with pretraining lesions of the ventromedial PFC exhibited impairments in recall of extinction when tested 24 hr after extinction training (Quirk et al., 2000). Previous studies have specifically implicated the activity of the infralimbic division of the mPFC (IL/mPFC) in the formation of extinction memory (Milad and Quirk, 2002; Burgos-Robles et al., 2009). Neurons in the IL/mPFC project to γ-aminobutyric acid (GABA)-releasing intercalated (ITC) neurons located between the basolateral (BLA) and central nuclei of the amygdala (CeA), providing feedforward inhibition of output neurons in the CeA (Royer et al., 1999). Activation of ITC neurons due to the increased firing of mPFC neurons may result in inhibition of the CeA, preventing conditioned fear responses (Likhtik et al., 2008; Amano et al., 2010). More recently, it has been demonstrated that neurons in both IL and prelimbic division of the mPFC (PL) exhibit increases in the firing rates during extinction recall (Holmes et al., 2012). It remains unknown, however, whether extinction is associated with synaptic plasticity in projections from the mPFC to the target structures in the amygdala.

Using ex vivo electrophysiology combined with optogenetic techniques (Boyden et al., 2005), we found that extinction learning was associated with reduced synaptic efficacy in projections from the mPFC to the BLA but unchanged synaptic transmission at mPFC inputs to ITC neurons. Furthermore, the balance between excitation and inhibition in the mPFC-BLA pathway was shifted toward inhibition after extinction. Moreover, the activation of mPFC projections inhibited excitatory transmission heterosynaptically in the auditory cortical inputs (auditory CS pathways) to the BLA. These plasticity mechanisms could contribute to the reduced expression of conditioned fear after extinction.

RESULTS

Selective Photostimulation of mPFC Projections to Amygdala

To investigate how the mPFC may influence the activity of amygdala, we transduced neurons in the mPFC of mouse brains with adeno-associated virus (AAV) vector coding ChR2(H134R)-eYFP

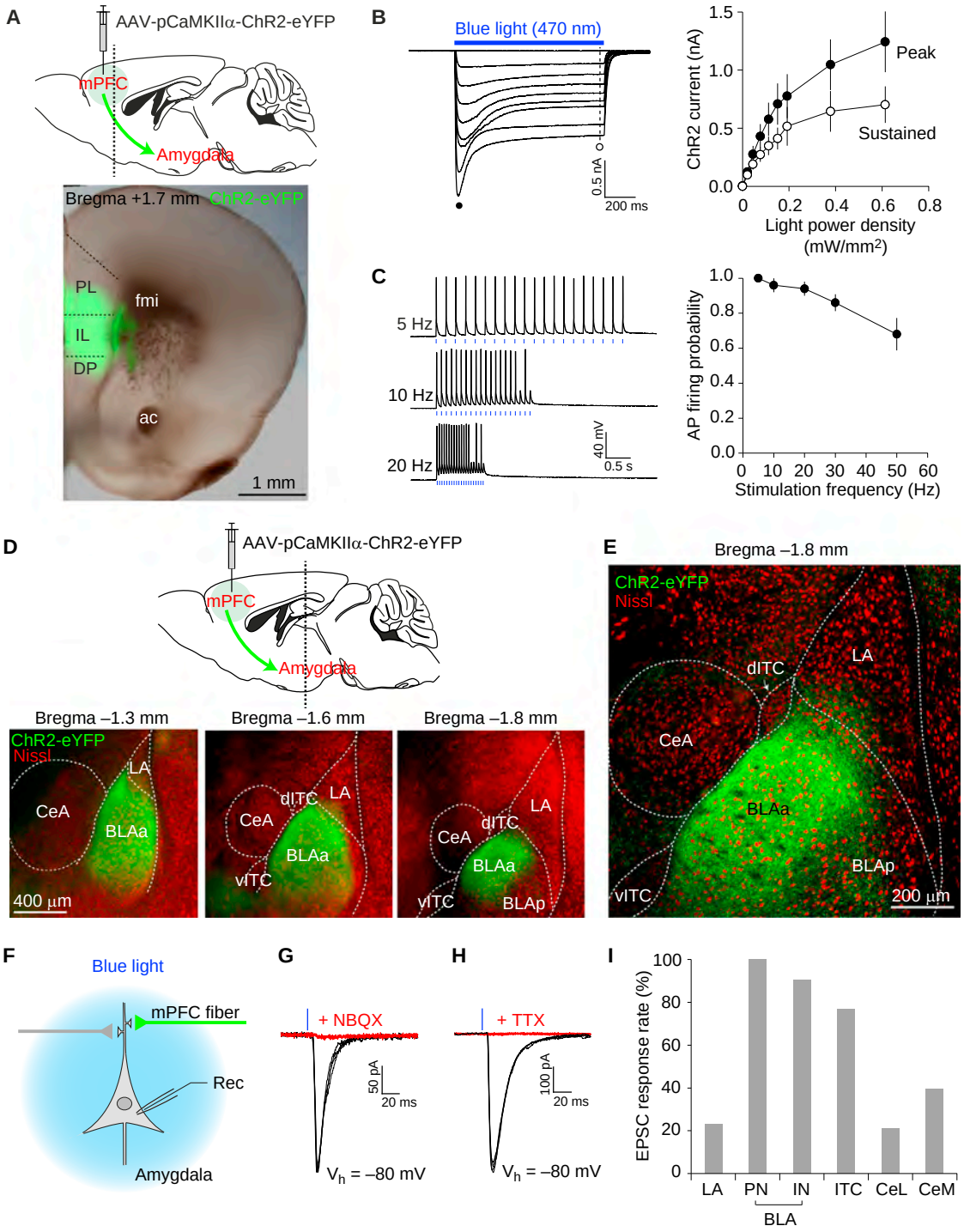

Figure 1. Optogenetic Projection-Specific Activation of mPFC Inputs to Amygdala

(A) Top: experimental design. A vertical line indicates location of the coronal section shown below. Bottom: expression of eYFP-tagged ChR2 in the mPFC (green). PL and IL, prelimbic and infralimbic divisions of the mPFC, respectively; DP, dorsal peduncular cortex; fmi, forceps minor of the corpus callosum; ac, anterior commissure.

(B) Left: ChR2-mediated currents in IL/mPFC neuron were evoked by 1 s pulses of light (470 nM, blue horizontal bar) with variable intensities (0.02–0.61 mW/mm^2) at –80 mV in voltage-clamp mode in the presence of NBQX (10 μM) and bicuculline (30 μM). Right: input-output curves of ChR2-mediated photocurrents showing peak (filled circles) and sustained current components (open circles) plotted as a function of light intensity (light power density, mW/mm^2, n = 4 neurons).

(C) Left: action potentials (APs) were evoked in a pyramidal neuron in the mPFC in current-clamp mode by 1 ms pulses of photostimuli at different frequencies (blue vertical lines). Right: summary plot of AP firing probability versus photostimulation frequency (n = 5 neurons).

(legend continued on next page)

fusion gene under control of the CaMKIIα promoter, placing the injection pipette tip into the IL/mPFC (but the spread of virus to PL has inevitably occurred, see below). Four weeks later, ChR2-eYFP, identified as green fluorescence, was abundantly expressed in the mPFC (Figure 1A). Illumination of the mPFC in slices with blue light (470 nm) resulted in inward currents in transduced IL neurons under voltage-clamp recording conditions at a holding potential of –80 mV (Figure 1B). Trains of short pulses (1 ms duration) of blue light induced action potential (AP) firing in ChR2-expressing neurons in current-clamp mode, which followed the frequency of photostimulation, confirming the functionality of expressed ChR2 (Figure 1C).

Axonal fibers originating from ChR2-eYFP-expressing projection neurons in the mPFC were identified as green fluorescence in coronal brain sections. These projections were found predominantly in the BLA, more specifically in its anterior subdivision (BLAa; Figures 1D and 1E). To a lesser extent, they were also observed in clusters of intercalated neurons (Royer et al., 1999). We determined whether the mPFC fibers make functional synapses onto neurons in the amygdala by examining the photostimulation-induced responses in these areas (Figure 1F; Figure S1 available online). In principal neurons in the BLA, short photostimuli (1 ms duration) evoked glutamatergic excitatory postsynaptic currents (EPSCs) under voltage-clamp conditions as evidenced by their sensitivity to the AMPA/kainate receptor antagonist NBQX (10 μM; Figure 1G). Synaptic responses were blocked by tetrodotoxin (TTX, 1 μM) (Figure 1H), confirming that they were due to AP firing in presynaptic fibers arising from the mPFC.

Photostimulation-induced EPSCs were observed in all principal neurons (PNs) examined (in total, 215 neurons) and most interneurons (90%, 74 out of 82 cells) within the BLAa. EPSCs could also be induced by photostimulation of the mPFC fibers in a large proportion of ITC neurons (77%, 112 out of 146 cells examined; Figure 1I), which are readily identifiable during recordings in slices, as they possess uniquely high input resistance (often >1.0 GOhm; Figures S1F and S1G). Photostimulation-induced EPSCs were less commonly detected in principal neurons of the lateral nucleus (LA; 23%, 3 out of 13 neurons) or lateral and medial divisions of the central nucleus of the amygdala (CeL or CeM, respectively; CeL: 21%, 4 out of 19 neurons; CeM: 39%, 13 out of 33 neurons; Figure 1I). Notably, polysynaptic inhibitory postsynaptic currents (IPSCs) with a delayed onset were induced by photostimulation of the mPFC fibers in nearly all neurons regardless of the nucleus examined (Figures S1A–S1E and S1H; also see below). These results indicate that mPFC neurons make extensive excitatory connections with specific nuclei of the amygdala.

The recorded EPSCs were monosynaptic as their latencies were relatively short, exhibiting small variability and unimodal distribution (Figures S2A and S2B). The EPSCs in the mPFC-BLA pathway were rescued by the application of 4-aminopyridine (4-AP), a blocker of voltage-gated K^+ channels, after they were blocked by tetrodotoxin, also indicating their monosynaptic origin (Figure S3; see Supplemental Text for details; Petreanu et al., 2009). Moreover, the decay times of EPSCs did not correlate with the EPSC amplitude or photostimulation intensity, and they were not different from decay times of purely monosynaptic EPSCs recorded in the presence of TTX and 4-AP (Figures S3H and S3I), suggesting that our EPSC recordings were not contaminated by polysynaptic contributions significantly. There were no differences between EPSC latencies recorded in neurons in different nuclei of the amygdala (LA, BLA, ITC, CeL, and CeM) (Figures S2H and S2J; $p = 0.94$).

Although we verified the location of AAV injection sites in the IL in each mouse tested, fluorescent signal was also found in the PL (Figure 1A), suggesting the spread of virus to this mPFC subdivision. To determine whether the IL and PL may project differently to the amygdala, we performed "angled" injections of the virus-containing solution into the IL to limit the spread of virus to the PL (Figures S4A, S5A, and S5C). In these experiments, the lack of photocurrents in PL neurons at different distances from the IL confirmed the locality of IL injections (Figure S4B). For the PL targeting, a straight angle injection was sufficient to attain localized ChR2 expression as potential backflow did not contaminate the IL (Figure S5B). We found that the projection patterns of IL or PL to the amygdala, when targeted separately, were essentially identical to the pattern observed with less localized injections (Figures S4C, S5B, and S5C). Photostimulation of either IL or PL projections resulted in robust monosynaptic EPSCs and disynaptic IPSCs in all BLAa neurons examined (Figures S4D, S4G, and S5D). There was no difference in EPSC/IPSC amplitude ratios between PL-BLA and IL-BLA projections (Figure S5D; $p = 0.54$), indicating that IL and PL neurons project to principal neurons and interneurons in the BLA identically. These results suggest that the patterns of IL-BLA and PL-BLA connectivity in mice might be similar. Moreover, photostimulation of IL projections induced EPSCs in ~70% of intercalated neurons tested (Figures S4F and S4G). This is also analogous to the mPFC-ITC connectivity estimates that we obtained with less localized AAV injections (Figure 1I).

Additionally, we assessed the mPFC-BLA connectivity using an alternative approach, injecting fluorescently labeled retrograde tracer (Katz et al., 1984) into the BLA. Within the mPFC, we found labeled neurons in layers 2 and 5 in both IL and PL (Figures S5E–S5G). We quantified the proportion of labeled neurons

(D) Top: experimental design. A vertical line indicates location of the coronal section through the amygdala. Bottom: microscopic images showing afferent fibers from the mPFC terminating in the BLA (green). BLAa and BLAp are anterior and posterior divisions of the BLA. dITC and vITC are dorsal and ventral clusters of ITC neurons. Red fluorescence indicates fluorescent Nissl stain.
(E) ChR2-eYFP-expressing mPFC fibers in the amygdala.
(F) Experimental set-up for recording of photostimulation-induced synaptic responses.
(G) Traces of light-evoked EPSCs recorded in a BLA principal neuron at –80 mV, blocked by NBQX (10 μM).
(H) EPSCs were also blocked by TTX (1 μM).
(I) Proportions of neurons in different nuclei of the amygdala that displayed EPSCs upon photostimulation of mPFC fibers at a given intensity (12.5 mW/mm^2). Numbers of neurons examined were 13, 215, 82, 146, 19, and 33 for LA, BLAa principal neurons (PN), BLAa interneurons (IN), ITC, CeL, and CeM, respectively. Error bars represent SEM.

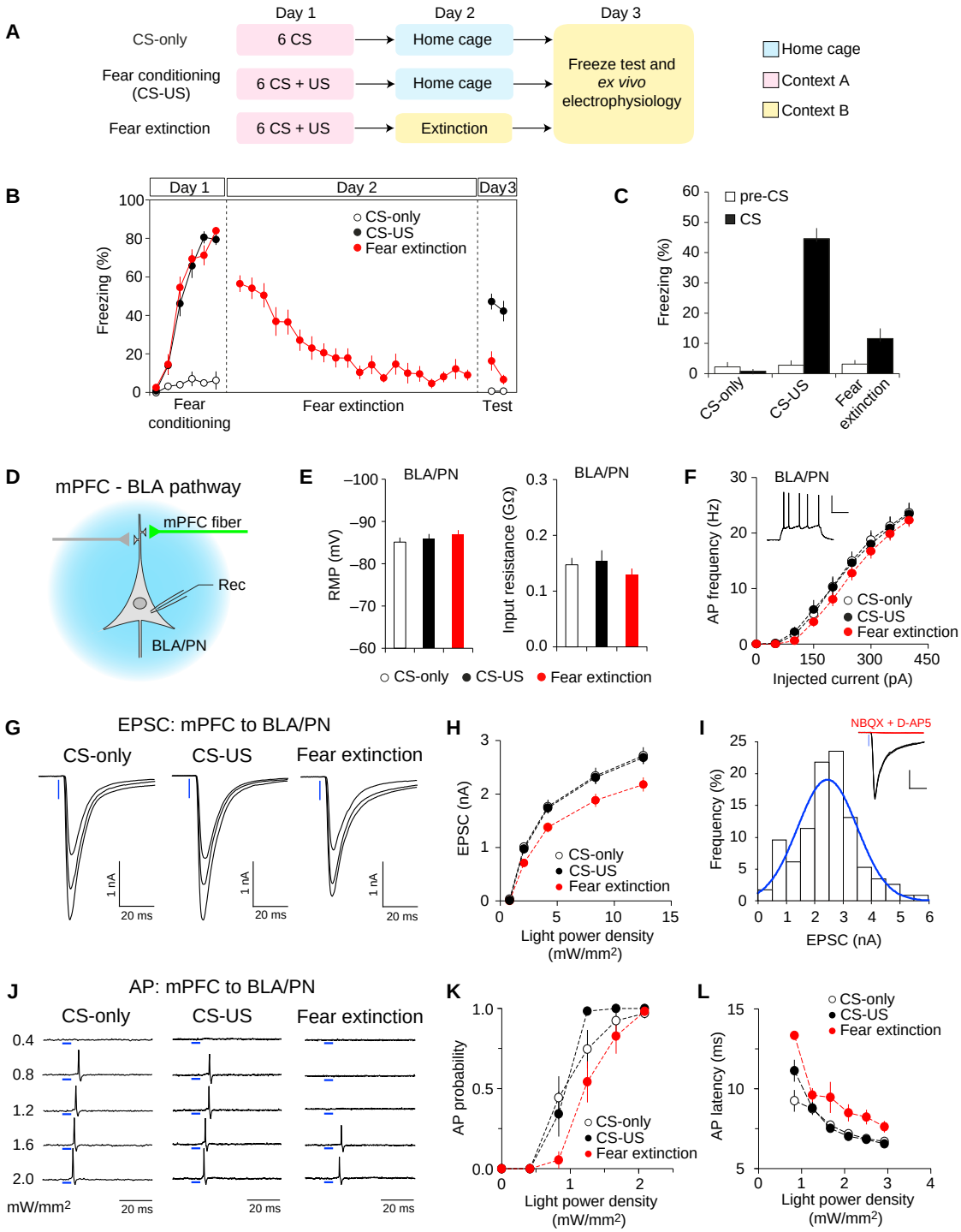

Figure 2. Extinction of Conditioned Fear Is Associated with Reduction of Excitatory Synaptic Strength in mPFC-BLA Pathway

(A) Design of fear conditioning and extinction experiments (CS-only group, n = 16 mice; CS-US, n = 22 mice; fear extinction, n = 21 mice).

(B) Freezing responses (% freezing) to the CS during different phases of the behavioral paradigm (fear conditioning, extinction, and test sessions).

(C) Freezing scores on the test day (day 3). For each mouse tested, freezing scores to two CSs were averaged.

(D) Experimental design. BLA/PN, BLA principal neuron.

(E) Resting membrane potential (RMP, left) and input resistance (R_{in}, right) in BLA principal neurons in different groups. R_{in} was calculated as in Figure S6A.

(F) Action potential (AP) frequencies in BLA/PN induced by 1 s current injections at –85 mV in current-clamp mode. Inset shows AP firing in BLA/PN (scale bars represent 0.4 s, 40 mV). n = 20 cells from 5 mice in each group for both (E) and (F).

(legend continued on next page)

to the total number of cells in layers 1–5 in different cortical areas and found that similar percentages of neurons in IL or PL were labeled with the retrograde tracer (Figure S5G; $p = 0.34$ between IL and PL). As the projection patterns of IL or PL to the amygdala were essentially indistinguishable and, most importantly, neurons in both IL and PL exhibit identical increases in the firing rates during extinction recall in mice (Holmes et al., 2012), we assayed the effects of behavioral training on mixed populations of IL and PL projections to the amygdala (as in Figure 1A).

Fear Extinction Is Associated with Decreased Excitatory Synaptic Efficacy in mPFC-BLA Projections

To explore synaptic mechanisms of fear extinction, we trained mice expressing ChR2 in the mPFC in the auditory fear conditioning paradigm (see Experimental Procedures; Figure 2A). Conditioned mice in the CS-US (fear conditioning) group exhibited much more freezing than control mice from the CS-only group during the fear memory test 48 hr postconditioning (Figures 2B and 2C; $p < 0.0001$, day 3). Mice in the extinction group, which were fear conditioned and subjected to extinction training the next day, showed significantly less freezing to CS presentations during the memory test on day 3 than mice in the CS-US group (Figures 2B and 2C; $p < 0.0001$). Pre-CS freezing levels did not differ between the groups (Figure 2C; $p = 0.91$).

The anterior subdivision of the BLA is more densely innervated by the mPFC fibers compared to other nuclei of the amygdala (Figures 1D and 1E). Therefore, we focused on the analysis of extinction-associated synaptic modifications in the mPFC-BLA pathway (Figure 2D). Passive membrane properties or excitability of principal neurons in the BLA remained unchanged after fear conditioning or extinction (Figures 2E and 2F; $p = 0.51$, 0.45, 0.06, and 0.53 for resting membrane potential, input resistance, AP frequency, and AP threshold potential, respectively). We recorded photostimulation-induced EPSCs in the BLAa principal neurons in slices from all behavioral groups, prepared immediately after the freezing test on day 3. Peak amplitudes of the mPFC-BLAa EPSCs followed a normal distribution at the same light intensity (12.5 mW/mm^2, Figure 2I; $p = 0.23$, Anderson-Darling normality test; CS-only and CS-US groups pooled together), suggesting that a population of recorded neurons was homogeneous in respect to the amplitude of EPSCs. We found that the input-output curves of EPSCs in the mPFC-BLA pathway were not different between CS-only and CS-US groups (Figures 2G and 2H; $p = 1.00$), whereas the input-output curve shifted to the right in slices from the fear extinction group compared to two other groups (Figures 2G and 2H; $p < 0.0001$ versus CS-only or CS-US groups). This finding indicates that fear extinction was accompanied by lasting reductions in excitatory synaptic efficacy in the mPFC-BLA pathway. The EPSC latencies in the mPFC-BLA pathway were unaffected by fear conditioning or extinction (Figures S2E and S2G; $p = 0.18$), suggesting that behavioral training did not change the monosynaptic nature of EPSCs in this pathway.

The magnitude of synaptic responses in the mPFC-BLA pathway was relatively large under our experimental conditions (Figures 2G–2I), potentially resulting in voltage errors during whole-cell recordings. However, we did not observe differences between behavioral groups in access resistance or membrane capacitance, which could promote steady-state and dynamic voltage errors (Figures S6A–S6C; $p = 0.83$ and 0.81, respectively). Moreover, the current-voltage (I-V) plots of AMPA receptor-mediated EPSCs (AMPAR EPSCs) were linear with the reversal potential close to 0 mV regardless of peak EPSC amplitudes in all groups (Figures S6D and S6F). Consistently, the ratio of the AMPAR EPSC amplitude at +40 mV to its amplitude at –80 mV was close to 0.5, the expected ratio based on linear I-V relationship for AMPAR-EPSC (Figures S6D and S6E). Moreover, the peak amplitude of EPSCs in the mPFC-BLA pathway was unaffected by the inhibitors of NMDA receptors, hyperpolarization-activated cyclic nucleotide-gated channels, or T-type and R-type voltage-dependent Ca^{2+} channels, which could be activated by large synaptic responses due to poor voltage- and space-clamp control (Figures S6G–S6I; $p = 0.88$, 0.71, and 0.36, respectively). Thus, these voltage-dependent conductances were unlikely to contaminate the peak amplitudes of EPSCs in our study. Moreover, we found that the probability of AP firing in BLA neurons in response to relatively weak photostimulation of mPFC projections was reduced in extinction group (Figures 2J and 2K; $p < 0.05$ and $p < 0.01$ versus CS-only and CS-US groups, respectively). The contribution of voltage errors was minimized in the latter experiments as APs were recorded in cell-attached mode. Notably, latency to photostimulation-induced AP firing was increased after fear extinction (Figure 2L; $p < 0.0001$ versus CS-only or CS-US group). This indicates that membrane depolarization of BLA neurons by synaptic activity in the mPFC-BLA projections might reach the threshold for AP generation more slowly in extinction group, providing further evidence for reduced excitatory postsynaptic responses in this pathway since passive membrane properties or excitability were not altered after fear extinction (Figures 2E and 2F).

The magnitude of paired-pulse ratio (PPR; 50 ms interpulse interval), a measure of presynaptic function (Zucker and Regehr, 2002), remained unaltered at the mPFC-BLA synapses in the CS-US group compared to the CS-only group (Figures 3A and 3B; $p = 1.00$). In contrast, PPR was increased in the extinction group compared to two other groups ($p < 0.05$ versus CS-only group and $p < 0.01$ versus CS-US), indicating the reduced probability of release (*Pr*). The I-V relations of either AMPA receptor

(G) EPSCs (averages of five responses) in the mPFC-BLA pathway in mice from all groups. EPSCs were induced by photostimuli of three different intensities.
(H) Input-output curves for peak amplitudes of EPSCs in the mPFC-BLA pathway. $p < 0.0001$ for EPSC amplitudes in fear extinction group (n = 61 cells from 15 mice) versus CS-only group (n = 54 cells from 10 mice) or versus CS-US mice (n = 61 cells from 15 mice).
(I) A distribution of peak amplitudes of EPSCs evoked by photostimulation (12.5 mW/mm^2) in the mPFC-BLA pathway. A fitted Gaussian curve (blue) is overlaid on the histogram. EPSCs were blocked by NBQX (10 μM) and D-AP5 (50 μM) (inset: scale bars represent 20 ms, 0.5 nA).
(J) Traces of AP firings induced by photostimulation of mPFC projections (5 ms pulses, blue bars). APs were recorded in BLA/PN in cell-attached mode.
(K) Probability of AP firing induced by photostimulation of mPFC projections. AP probability at each light intensity was determined after five to ten trials.
(L) The latency to AP firing versus photostimulation intensity. n = 13–14 cells from 5 mice in each group for both (K) and (L). Error bars represent SEM.

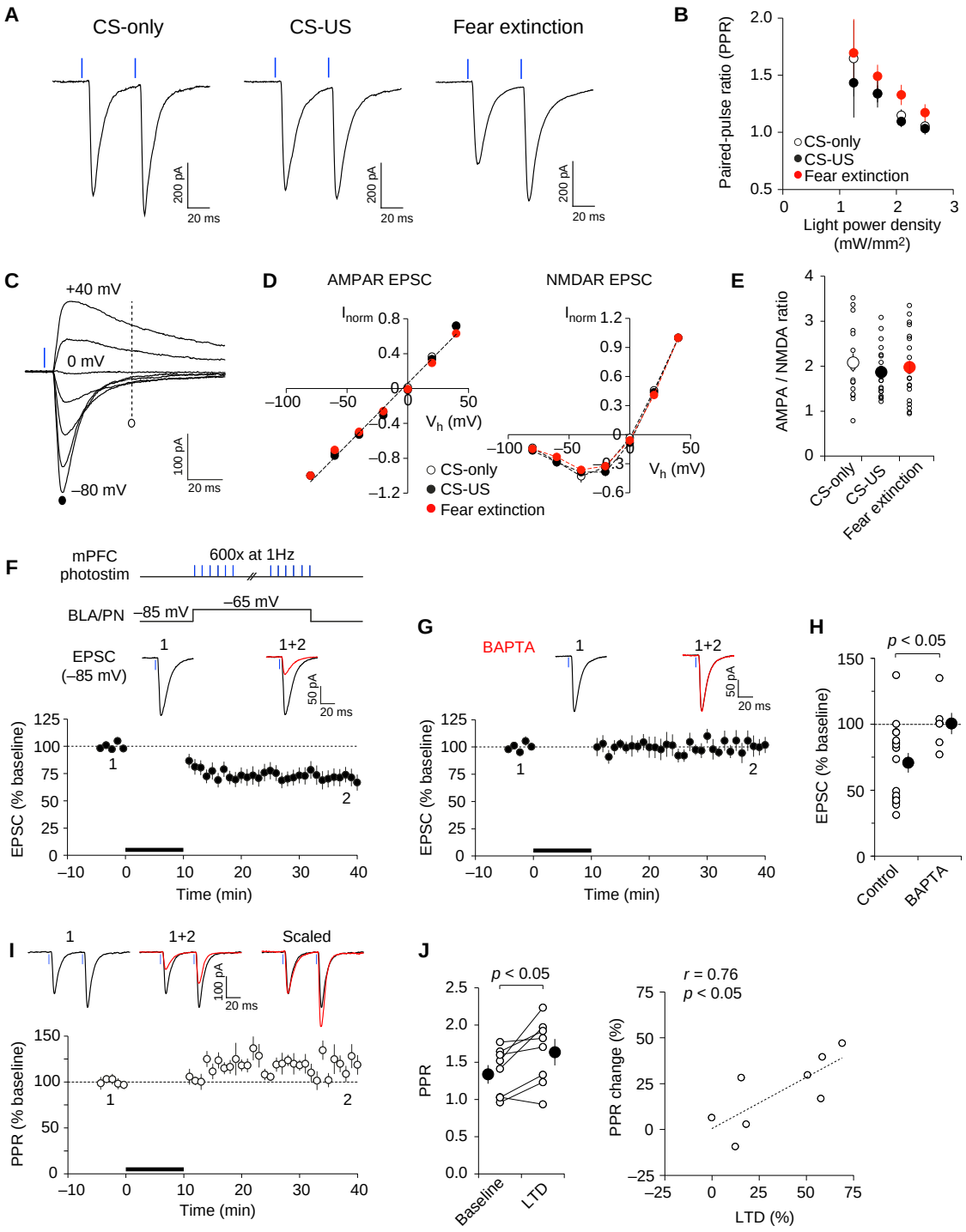

Figure 3. Mechanisms of Fear Extinction-Associated Depression of Synaptic Transmission in mPFC-BLA Pathway

(A) EPSCs evoked in BLA principal neurons by paired photostimuli (2.5 mW/mm^2; 50 ms interpulse interval) in slices from all groups.

(B) PPR in extinction group (n = 22 cells from 10 mice) was larger than in CS-only (n = 21 cells from 7 mice) or CS-US groups (n = 28 cells from 9 mice).

(C) Photostimulation-induced EPSCs in a BLA principal neuron at holding potentials ranging from –80 mV to +40 mV in the presence of bicuculline (30 μM).

(D) Current-voltage (I-V) plots of EPSCs in the mPFC-BLA pathway. Left: the amplitude of AMPAR EPSC was measured at the peak (marked with a filled circle in C). Right, the amplitude of NMDAR EPSCs was measured at 50 ms after the photostimulus (marked with an open circle in C). AMPAR-EPSCs and NMDAR EPSCs at different holding potentials were normalized to EPSCs recorded at –80 mV or +40 mV, respectively (I_{norm}). n = 15, 24, and 26 cells from 6, 8, and 8 mice for CS-only, CS-US, and fear extinction groups, respectively.

(legend continued on next page)

(AMPAR)- or NMDA receptor (NMDAR)-mediated EPSCs were not different between behavioral groups (Figures 3C and 3D; $p = 0.36$ and $p = 0.97$ for AMPAR and NMDAR EPSCs, respectively). Moreover, AMPAR/NMDAR EPSC amplitude ratio was also not different between groups (Figure 3E; $p = 0.60$), indicating that neither fear conditioning nor extinction had an effect on postsynaptic function in the mPFC-BLA pathway. These findings suggest that fear extinction-associated reductions in excitatory synaptic transmission in the mPFC-BLA pathway might be due to the decreased *Pr*.

We also found that long-term depression (LTD) could be induced at the mPFC-BLA synapses. Thus, photostimulation of ChR2-expressing mPFC fibers at a frequency of 1 Hz for 10 min with mild depolarization of postsynaptic neurons resulted in significant depression of light-induced EPSCs in BLA neurons (Figures 3F and 3H). The induction of LTD was prevented when a high affinity Ca^{2+} chelator BAPTA (10 mM) was included in the recording pipette solution (Figures 3G and 3H). LTD was accompanied by an increase in PPR (Figures 3I and 3J; $p < 0.05$), and the magnitude of LTD correlated positively with PPR changes (Figure 3J; $r = 0.76$, $p < 0.05$), indicating that LTD under given conditions was, at least in part, presynaptically expressed. Thus, LTD induced in slices may be mechanistically similar to reductions in excitatory synaptic efficacy in prefrontal projections to the BLA after fear extinction. These results suggest an interesting possibility that LTD-like mechanisms may underlie extinction-associated synaptic changes in the mPFC-BLA pathway.

Balance between Excitation and Inhibition in mPFC-BLA Pathway Is Shifted after Fear Extinction

The strength of GABA receptor A ($GABA_AR$)-mediated inhibition in the BLA may control extinction of conditioned fear memory (Myers and Davis, 2007). Therefore, we asked whether activation of mPFC fibers projecting to the BLA results in feedforward inhibition of BLA neurons (Figure 4A), and, if so, how it is affected by fear extinction. Photostimulation of the mPFC fibers induced excitatory postsynaptic potentials (EPSPs) in a current-clamp mode in a majority of recorded BLA interneurons (Shin et al., 2006) (Figure 4B). Stronger intensities of photostimulation were often sufficient to drive the AP firing in recorded cells (Figures 4B and 4C; in 10 of 20 interneurons tested). Thus, projections from the mPFC make direct excitatory connections on BLA interneurons. Accordingly, photostimulation of the mPFC fibers induced biphasic synaptic responses in principal neurons, comprised of the early EPSC and delayed IPSC at depolarized membrane potentials (Figures 4D and 4E). The EPSCs and IPSCs could be recorded in isolation when synaptic currents were evoked at –80 mV or 0 mV (Figure 4F), which are close to the reversal potential for the IPSC (–71.5 mV, estimated from I-V plots of isolated IPSCs) or the EPSC (0 mV; Figure 3D), respectively. The $GABA_AR$ antagonist bicuculline (30 μM) suppressed synaptic currents recorded at 0 mV, whereas peak amplitudes of synaptic currents at –80 mV were unaffected, indicating the lack of cross-contamination between EPSCs and IPSCs at these holding potentials (Figure 4F). The joint application of NBQX (10 μM) and NMDAR antagonist D-AP5 (50 μM) inhibited both EPSCs and IPSCs (Figure 4G), providing evidence of disynaptic nature of IPSCs recorded in BLA neurons. Consistent with this possibility, synaptic latencies of IPSCs in the mPFC-BLA pathway were much longer compared to EPSCs in the same projections or EPSCs in inputs to the BLA from the auditory cortex (Figure 4H, $p < 0.0001$; also Figures S2B–S2D). Thus, activation of BLA interneurons by the mPFC fibers contributes to feedforward inhibition of principal neurons in the BLA. It appears that local inhibitory interneurons, activated by inputs from the mPFC, prevented polysynaptic EPSCs in BLA principal neurons, as the application of bicuculline led to the appearance of polysynaptic EPSC components (Figures 4I). However, we found that the EPSCs in interneurons, induced by photostimulation of projections from the mPFC, often displayed more than one peak, even in the absence of bicuculline, probably reflecting both monosynaptic (first peak) and disynaptic (second peak) EPSCs (Figures S7A–S7C). Moreover, photostimulation of mPFC projections sometimes resulted in IPSCs in BLA principal neurons with clear double peaks (Figure S7D). The latter observation probably reflected the presence of trisynaptic feedback inhibitory responses in BLA neurons (Figure S7B). Consistently, the decay time constant of IPSCs was positively correlated with photostimulation intensity in all groups (Figures S7I and S7J; $p < 0.001$), and IPSCs induced by relatively strong photostimulation (4–12.5 mW/mm^2) displayed larger decay time constants compared to monosynaptic IPSCs induced in the BLA/IN-BLA/PN pathway (Figures S7I and S7J; $p < 0.05$), suggesting a contribution of feedback inhibition. To avoid the contamination of feedforward IPSCs by feedback inhibitory components, we defined a time window that could allow for a relatively selective detection of feedforward IPSCs. We estimated the latency of feedback IPSCs by calculating the latencies of AP firing and IPSCs in each component of trisynaptic feedback inhibitory circuit (Figures S7E–S7H). Based on these estimates, we set the time window for detection of peak amplitudes of feedforward IPSCs as the time interval between 8 and 12 ms after the onset of

(E) AMPAR/NMDAR EPSC amplitude ratios, calculated as the ratio of peak amplitude of AMPAR EPSC at –80 mV to NMDAR EPSC amplitude at +40 mV. Small symbols show data from individual neurons, whereas larger circles represent average values.
(F) Top: a protocol for the induction of LTD. To induce LTD, the recorded BLA principal neuron was depolarized from a baseline holding potential to –65 mV and presynaptic mPFC inputs were photostimulated (1 ms) at 1 Hz for 10 min (black bar in a lower graph). Bottom: time course of EPSC amplitude changes. Traces are the averages of 10–15 EPSCs recorded before (1) and 25–30 min after (2) LTD induction. n = 16 neurons from 12 mice.
(G) LTD was blocked when BAPTA (10 mM) was included in the pipette solution (n = 6 neurons from 4 mice).
(H) Summary of LTD experiments as in (F) and (G).
(I) mPFC-BLA EPSCs evoked in BLA neurons by paired photostimuli (50 ms interval) before (1) and after (2) LTD induction. Below, the time course of PPR changes (normalized to the average baseline PPR). n = 8 neurons from 7 mice.
(J) Left: PPR changes after the induction of LTD. n = 8 neurons from 7 mice. Right: PPR changes correlated positively with the magnitude of LTD. Error bars represent SEM.

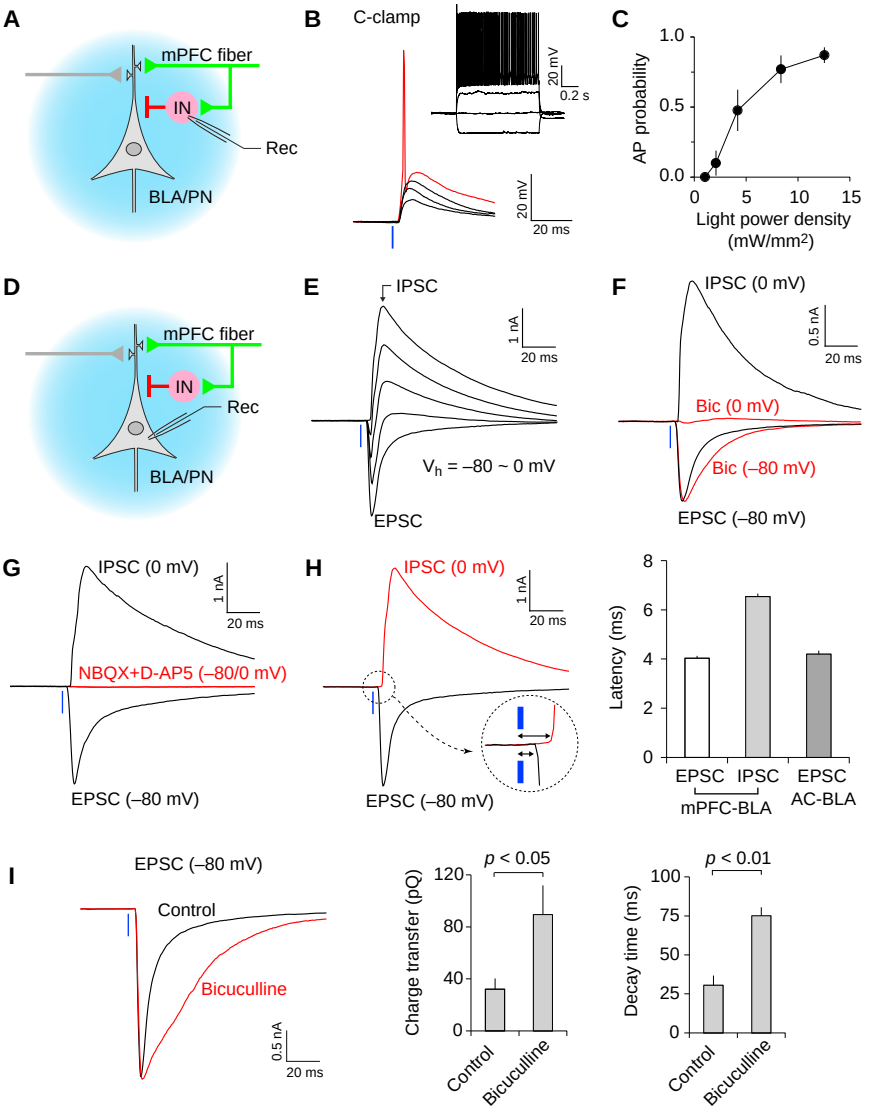

Figure 4. Activation of mPFC Afferents Leads to Feedforward Inhibition of BLA Principal Neurons

(A) Experimental design for recording of light-evoked (blue) synaptic responses in local circuit interneurons (IN) in the BLA.

(B) BLA interneuron exhibits nonaccommodating AP firing (inset). Synaptic responses were induced in BLA interneuron by photostimulation of mPFC projections in current-clamp mode with stronger light intensities resulting in AP firing (red trace).

(C) Probability of AP firing in BLA interneurons in response to photostimulation of the mPFC projections. It was assayed in cell-attached or current-clamp modes at resting membrane potential (n = 10 neurons).

(D) Experimental design for recording of the light-evoked EPSC/IPSC in BLA principal neurons (BLA/PN).

(E) The EPSC/IPSC in a BLA/PN at holding potentials ranging from –80 mV to 0 mV.

(F) Synaptic currents recorded at 0 mV were completely blocked by $GABA_A$ receptor antagonist bicuculline (30 μM, Bic; red trace at 0 mV). However, the peak amplitude of synaptic currents at –80 mV was not affected by bicuculline (red trace at –80 mV).

(G) Both EPSC and IPSC (recorded at –80 mV or 0 mV, respectively) were blocked by jointly applied NBQX (10 μM) and D-AP5 (50 μM) (red traces at –80 mV and 0 mV).

(H) Left: synaptic latency analysis for EPSCs and IPSCs recorded in BLA/PN. Right: synaptic latency of IPSCs in the mPFC-BLA pathway (n = 19 cells) was significantly longer compared to photostimulation-induced EPSCs (n = 22 cells) or EPSCs induced by electrical stimulation of inputs to the BLA from the auditory cortex (AC, n = 21 cells).

(I) Left: photostimulation-induced EPSCs in a BLA/PN (12.5 mW/mm^2, 1 ms duration) under control conditions (black trace) and in the presence of bicuculline (30 μM, red trace). Right: average total charge transfer and 90%-to-10% decay time of EPSCs recorded in the presence or absence of bicuculline (n = 6 neurons from 4 mice). Error bars represent SEM.

photostimulation. We carefully examined our IPSC recordings within this window, excluding trisynaptic (delayed) components from the analysis.

To determine whether fear extinction affects feedforward inhibitory circuitry in the mPFC-BLA pathway, we first compared EPSCs recorded in local interneurons in the BLA (BLA/IN), induced by photostimulation of mPFC projections, between behavioral groups (Figure 5A). Notably, passive membrane properties or excitability in BLA interneurons were unchanged by behavioral training (Figures 5B and 5C; p = 0.87, 0.07, 0.25, and 0.67 for resting membrane potential, input resistance, AP frequency, and AP threshold potential, respectively). EPSCs in the mPFC-BLA/IN pathway were monosynaptic as the application of 4-AP rescued TTX-blocked EPSCs (Figure S3F). There was no significant difference in synaptic input-output curves for EPSCs in the mPFC-BLA/IN pathway between behavioral groups (Figures 5D and 5E; p = 0.42). Consistently, we did not detect any differences in the probability of AP firing in BLA/IN in response to photostimulation of mPFC fibers between groups (Figures 5F and 5G; p = 0.48). These results suggest that fear conditioning or extinction had no effect on synaptic efficacy or AP firing output in the mPFC-BLA/IN pathway. Next, we examined whether fear conditioning or extinction could affect inhibitory synaptic responses from BLA/IN to BLA/PN. To record IPSCs in the BLA/IN to BLA/PN pathway, we used electrical stimulation of BLA/IN with electrodes placed onto the BLA in the presence of NBQX and D-AP5 (Figure 5H). Synaptic responses recorded in these experiments in BLA neurons were blocked by bicuculline (Figure 5H), confirming that they were GABAergic IPSCs. To minimize voltage-clamp errors associated with large IPSCs, we used the pipette solution with a high Cl^- concentration ($[Cl^-]_{in}$ = 132 mM). This shifted the reversal potential of IPSCs to approximately –15 mV (Figure 5I), thus resulting in smaller IPSC amplitudes at 0 mV compared to IPSCs recorded

with low $[Cl^-]_{in}$ (12 mM) in previous experiments (Figures 4D–4H). Recorded IPSCs displayed linear I-V relations with no differences in the reversal potential between groups (Figure 5I; p = 0.27). We found that the amplitude of IPSCs recorded in BLA/PN were not different between groups (Figures 5J and 5K; p = 0.34), suggesting that inhibitory synaptic efficacy in the BLA/IN to BLA/PN pathway remained unaltered after fear conditioning or extinction. In agreement with these results, the input-output curves or synaptic latencies for feedforward IPSCs in the mPFC-BLA/IN-BLA/PN pathway were not different between groups, either (Figures 5L–5N, p = 0.50 for IPSC amplitudes; Figures S2F and S2G; p = 0.80 for IPSC latencies), indicating that behavioral training had no effect on feedforward inhibition in this pathway. Notably, we did not detect differences in IPSCs induced by weak photostimulation (2 mW/mm^2) between groups (Figure 5N; p = 0.98). The decay time constant of these IPSCs was similar to that of monosynaptic IPSCs (Figures S7I and S7J; p = 1.00), suggesting that these inhibitory synaptic responses mainly reflected feedforward inhibition with little contamination by feedback IPSCs. As the extinction-associated reduction in synaptic efficacy was restricted to excitatory synapses in the mPFC-BLA/PN pathway (Figure 2), the balance between excitation and inhibition in projections from the mPFC to the BLA would be shifted toward inhibition after fear extinction.

Priming Stimulation of mPFC Afferents Leads to Heterosynaptic Inhibition in Auditory Cortical Inputs to BLA

As the mPFC projections activate BLA/IN (see Figure 4), CS-induced increases in the mPFC activity would, in turn, lead to enhanced feedforward inhibition of BLA neurons. The activity-driven accumulation of GABA was shown to induce a transient suppression of glutamatergic synaptic transmission at CS inputs to the amygdala via activation of presynaptic $GABA_B$ receptors (Shaban et al., 2006). Thus, we addressed a possibility of GABA-mediated interactions between convergent inputs from the auditory CS areas (auditory cortex, AC) and mPFC to the BLA (Figure 6A). Short trains of photostimuli to mPFC fibers (3 pulses, 50 ms interpulse intervals) resulted in both monosynaptic EPSCs and disynaptic IPSCs in BLA principal neurons recorded at –80 mV and 0 mV, respectively (Figure 6B). We induced EPSCs in the AC-BLA pathway, delivering electrical stimuli to the external capsule, with variable delays after photostimulation of the mPFC afferents. The amplitude of EPSCs in the AC-BLA pathway, induced shortly after the priming mPFC stimulation, was significantly reduced compared to baseline EPSCs without mPFC stimulation (Figure 6C). This heterosynaptic inhibition of the EPSCs in the AC-BLA pathway was most prominent with shorter delays between activation of mPFC fibers and stimulation of the AC-BLA pathway, but it could still be observed when the interval was as long as 800 ms (Figures 6C and 6E; p < 0.001). Inhibition could also be observed after a single priming photostimulus, but it was significantly more pronounced when three photostimuli were delivered to the mPFC fibers (35% ± 4% and 24% ± 4% inhibition for a train or a single pulse priming, respectively, n = 10 neurons, p < 0.01). The magnitude of heterosynaptic inhibition by activation of IL/mPFC fibers was similar to that found with less localized expression of ChR2 in the mPFC (Figure S4E). The observed decrease in the EPSC amplitude was accompanied by increases in PPR (Figures 6D and 6F; p < 0.001), which were positively correlated with the magnitude of inhibition (Figure 6G; r = 0.76, p < 0.001). These indicate that heterosynaptic inhibition in the AC-BLA pathway was due to reduced glutamate release (Zucker and Regehr, 2002). Furthermore, the magnitude of heterosynaptic inhibition also correlated with priming IPSC amplitudes in the mPFC-BLA projections (Figure 6H; r = 0.41, p < 0.05), suggesting the role for GABA, released from BLA interneurons in response to activation of the mPFC fibers, in this form of short-term synaptic plasticity.

Heterosynaptic inhibition at the AC-BLA synapses after priming photostimulation of the mPFC fibers was not observed in the presence of the $GABA_B$ receptor antagonist CGP 52432 (10 μM) (Figures 6I and 6J; p = 0.08 versus no mPFC priming; p < 0.001 versus experiments without antagonist). PPR changes were also prevented by CGP 52432 (Figure 6K; p = 0.78 versus no mPFC priming; p < 0.001 versus experiments without antagonist). This indicates that heterosynaptic inhibition in the AC-BLA pathway was mediated by activation of presynaptic $GABA_B$ receptors by GABA released during priming stimulation of the mPFC fibers.

Moreover, heterosynaptic inhibition in the AC-BLA pathway was enhanced in the fear extinction group compared to the CS-only or CS-US groups (Figures 6L and 6M; p < 0.001 and p < 0.05, respectively). PPR changes, associated with heterosynaptic inhibition, were also more prominent in the fear extinction group (Figure 6N; p < 0.01 versus CS-only group, p < 0.05 versus CS-US group). We found that heterosynaptic inhibition of EPSCs in the AC-BLA pathway was induced by priming stimulation of mPFC fibers with the EPSC amplitude as small as 120 pA, not inducing AP firing in BLA neurons (Figure S8). This finding indicates that heterosynaptic inhibition in the auditory CS pathway could be induced by priming mPFC activation at the subthreshold intensities of photostimulation, suggesting that the observed heterosynaptic interactions might be functionally relevant.

Intercalated Neurons in Amygdala Receive Direct Projections from mPFC

Whereas previous studies provided support to the notion that the IL/mPFC may control the activity of intercalated (ITC) neurons (Quirk et al., 2003; Amir et al., 2011), contributing to suppression of conditioned fear responses, it has not been unequivocally determined whether ITC neurons receive direct excitatory inputs from the mPFC. To address this question, we expressed ChR2 in the mPFC, including its IL division, and performed whole-cell patch-clamp recordings from ITC neurons. The ChR2-expressing mPFC fibers were detected in both dorsal (dorsolateral) and ventral (ventromedial) clusters of ITC neurons (dITC and vITC, respectively; Figure 7A), although to a lesser extent than in the BLA (Figures 1D and 1E). Photostimulation of mPFC fibers induced EPSCs in a large fraction of ITC neurons (77%, 112 out of 146 recorded cells; Figure 7B). However, the amplitude of photostimulation-induced EPSCs in ITC neurons was much smaller compared to EPSCs in inputs to BLA principal neurons (Figure S1I). EPSCs recorded in ITC neurons were blocked by NBQX (10 μM; Figure 7B), confirming their glutamatergic nature.

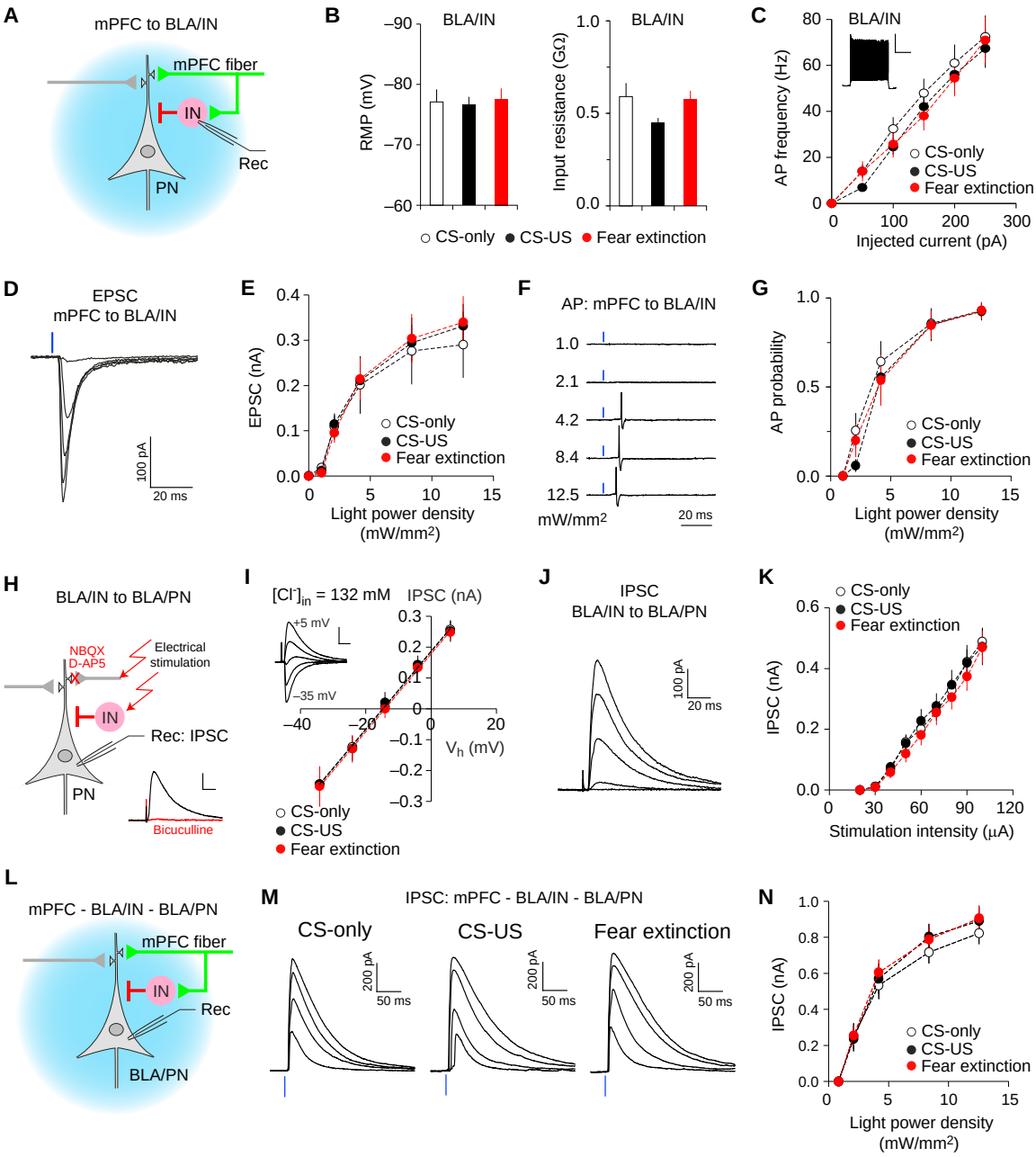

Figure 5. Fear Extinction Is Not Associated with Changes in Feedforward Inhibitory Circuits in the mPFC-BLA Pathway

(A) Design for recording EPSCs in the mPFC-BLA interneuron (BLA/IN) pathway.

(B) Resting membrane potential (RMP) and input resistance in BLA/IN. Input resistance was calculated as in Figure S6A.

(C) AP firing frequencies in BLA/IN in different groups. AP firing was induced as in Figure 2F. Inset, an example of AP firing (scale bars represent 0.4 s, 40 mV). n = 20, 26, and 24 cells from 5 mice each in CS-only, CS-US, and fear extinction groups, respectively for both (B) and (C).

(D) EPSCs in BLA/IN at –85 mV, induced by photostimulation of mPFC projections at different light intensities (blue bar).

(E) Peak amplitudes of monosynaptic EPSCs in BLA/IN versus photostimulation intensity. n = 14, 16, and 17 cells from 5 mice each in CS-only, CS-US, and fear extinction groups, respectively.

(F) Traces of AP firings evoked by photostimulation of mPFC projections (1 ms long) at different light intensities. AP firings were recorded in BLA/IN in cell-attached mode or in current-clamp mode at resting membrane potential.

(G) A plot of AP firing probability versus photostimulation intensity. AP probability at each photostimulation intensity was calculated after five trials. n = 14, 12, and 10 cells from 7, 5, and 4 mice for CS-only, CS-US, and fear extinction groups, respectively.

(H) Experimental design for recording of IPSCs in the BLA/IN to BLA/PN pathway. IPSCs in BLA/PN were induced by electrical stimulation with an electrode placed onto the BLA in the presence of NBQX (10 μM) and D-AP5 (50 μM) and were recorded at 0 mV in voltage-clamp mode. Cs^+-based pipette solution with

(legend continued on next page)

These EPSCs exhibited short synaptic latencies, which did not differ from the EPSC latencies in the mPFC-BLA pathway ($p = 0.96$; Figure 7B). Rescue of TTX-blocked EPSCs by 4-AP in ITC neurons indicates their monosynaptic origin (Figure S3G). These results show that projections from the mPFC activate ITC neurons through direct excitatory inputs.

The proportion of ITC neurons displaying EPSCs in response to photostimulation of the mPFC fibers at a given light intensity (12.5 mW/mm^2) did not differ between behavioral groups (74%, 82%, and 73% for CS-only, CS-US and extinction groups, respectively; $p = 0.46$, χ^2 test; n = 39, 56, and 51 neurons from 9, 14, and 14 mice for CS-only, CS-US, and extinction groups, respectively). The synaptic input-output curves for the EPSCs recorded in dITC or vITC were also unaffected by behavioral training (Figures 7C and 7D; $p = 0.56$ and $p = 0.98$ for dITC and vITC, respectively). Furthermore, there was no difference in the I-V relationships of AMPAR- and NMDAR-mediated EPSCs between the groups (Figures 7E and 7F; $p = 0.85$ for AMPAR EPSC, and $p = 0.99$ for NMDAR EPSC). The AMPAR/NMDAR EPSC ratios were also very similar in the CS-only, CS-US, and extinction groups (Figure 7G; $p = 0.97$), indicating the lack of postsynaptic modifications. These results show that the excitatory synaptic efficacy in projections from the mPFC to ITC neurons remained unaltered after fear conditioning or fear extinction.

Consistent with a sparse distribution of excitatory projections from the mPFC within the CeA (Figure 7H), photostimulation-induced monosynaptic EPSCs were observed in only a fraction of CeM neurons (39%, 13 out of 33 neurons). Conversely, activation of ChR2-expressing mPFC fibers induced large IPSCs in most recorded CeM cells (97%, 30 out of 31 CeM neurons examined; Figure 7I and Figure S1H). Moreover, the EPSC/IPSC amplitude ratio was substantially smaller in CeM neurons compared to BLA principal neurons or ITC neurons (Figure 7J; $p < 0.0001$ and $p < 0.01$ versus BLA neurons and ITC neurons, respectively), indicating that inhibitory responses predominate in the CeM when mPFC fibers are activated. Synaptic latencies of IPSCs in CeM neurons were much longer compared to monosynaptic EPSCs recorded in the CeM or other nuclei of the amygdala (Figure 7I and Figures S2I and S2J), suggesting their polysynaptic origin. While activation of GABAergic neurons in the CeL or CeM may contribute to IPSCs in the CeM, ITC neurons are the more likely source of the CeM IPSCs during mPFC stimulation because the proportion of ITC neurons with direct excitatory inputs from the mPFC is much larger compared to CeL or CeM neurons (Figure 1I; $p < 0.001$, χ^2 test). Moreover, the EPSC/IPSC amplitude ratio is larger in ITC neurons than in CeL or CeM neurons (Figure S1J; $p < 0.05$), indicating that ITC neurons would be more readily activated by excitatory inputs from the mPFC. Our findings show that activation of mPFC fibers results in robust inhibitory synaptic responses in CeM neurons, possibly due to recruitment of the mPFC-ITC-CeM pathway. This could lead to enhanced inhibition of CeM neurons by increased mPFC activity during extinction recall (Milad and Quirk, 2002; Holmes et al., 2012), thus suppressing conditioned fear response.

DISCUSSION

Combining optogenetic techniques with electrophysiological recordings in slices from behaviorally trained mice, we demonstrated that extinction of conditioned fear memory is associated with synaptic reductions in glutamatergic projections from the mPFC to principal neurons in the BLA (Figure 8). Whereas afferent fibers originating in the mPFC form excitatory synapses on both principal neurons and local circuit interneurons, the amplitude of monosynaptic EPSCs in the mPFC-BLA/IN pathway or disynaptic GABAergic IPSCs in the mPFC-BLA/IN-BLA/PN pathway remained unchanged after extinction training, thus shifting the excitation/inhibition balance in these projections to favor inhibition. Moreover, priming stimulation of mPFC resulted in heterosynaptic inhibition at inputs to the BLA from the auditory CS areas, which is enhanced in fear-extinguished animals. Finally, the synaptic efficacy at direct inputs from the mPFC to ITC neurons, inhibiting the CeM, the output nucleus of the amygdala, was retained after extinction learning. These multiple synaptic mechanisms could contribute to the extinction-associated suppression of conditioned fear responses for the reasons discussed below.

Neural activity in the IL/mPFC is increased during recall of extinction memory (Milad and Quirk, 2002), which is possibly mediated by the enhanced membrane excitability and LTP-like plasticity at glutamatergic inputs to mPFC neurons (Herry and Garcia, 2002; Santini et al., 2008; Vouimba and Maroun, 2011). More recently, the increased neuronal firing rates were demonstrated in both IL and PL during retrieval of extinction memory in mice (Holmes et al., 2012). The latter observation is consistent with our results, providing evidence for very similar projection patterns from IL or PL to the BLA in the mouse brain. This notion is supported by previous studies demonstrating that IL as well as PL project to the BLA (Takagishi and Chiba, 1991; Gabbott

high $[Cl^-]_{in}$ (132 mM) was used in experiments shown in (H)–(K). The IPSC (black trace, inset) was blocked by 30 μM bicuculline (red trace). Scale bars represent 20 ms, 50 pA.

(I) I-V plots for IPSCs (evoked as in H) were similar in all groups. Inset: IPSCs in the BLA/IN-BLA/PN pathway at V_h ranging from –35 mV to +5 mV (scale bars represent 20 ms, 100 pA). n = 9–11 cells from 3–4 mice in each group.

(J) IPSCs in the BLA/IN-BLA/PN pathway at different stimulation intensities. IPSCs were induced by electrical stimulation of the BLA and recorded in BLA/PN at 0 mV in voltage-clamp mode.

(K) A plot of peak amplitudes of IPSCs in the BLA/IN-BLA/PN pathway versus stimulation intensity. n = 16–18 cells from 5 mice in each group.

(L) Experimental design for recording of feedforward inhibition in the mPFC-BLA/IN-BLA/PN pathway.

(M) IPSCs recorded in BLA/PN in different groups. IPSCs were recorded in BLA/PN at 0 mV in voltage-clamp mode with Cs^+-based pipette solution containing high $[Cl^-]_{in}$ (132 mM).

(N) A plot of peak amplitudes of feedforward IPSCs (as in M) versus photostimulation intensity. The time window for detection of peak amplitudes was set as the time interval between 8 and 12 ms after the onset of photostimulation (see Figures S7E–S7H for details). n = 15–16 cells from 4 mice in each group. Error bars represent SEM.

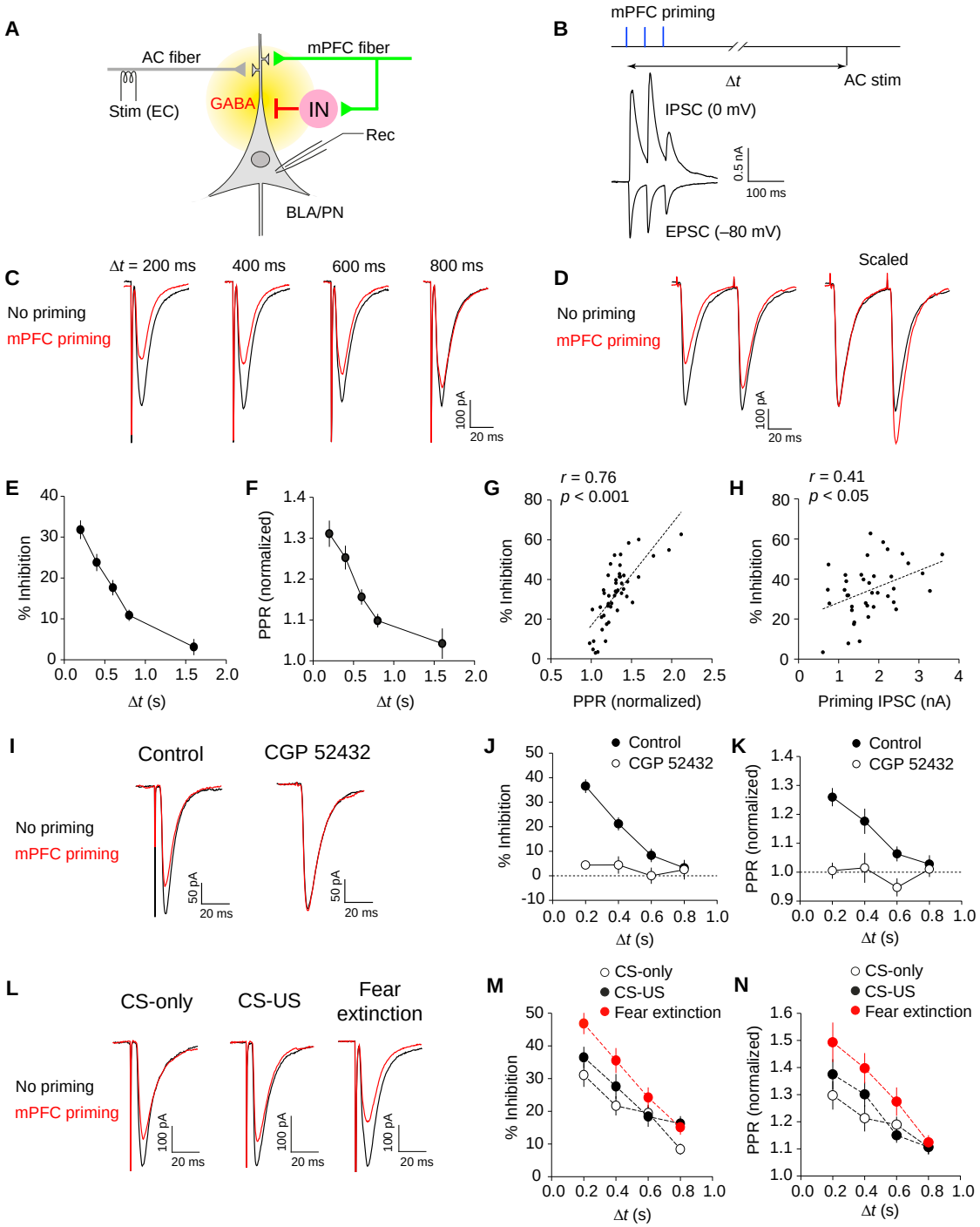

Figure 6. Priming Stimulation of mPFC Fibers Induces Heterosynaptic Inhibition in the AC-BLA Pathway

(A) Experimental design. Afferent fibers originating in the auditory cortex (AC) were stimulated electrically with an electrode placed onto the external capsule (EC), whereas ChR2-expressing mPFC fibers were stimulated with blue light. Synaptic responses were recorded in BLA/PN.

(B) Coactivation of mPFC and AC fibers. Three priming photostimuli (50 ms interpulse intervals), delivered to mPFC fibers, preceded electrical stimulation of the AC-BLA pathway with variable time intervals (Δt). Bottom traces show monosynaptic EPSCs and disynaptic IPSCs recorded in a BLA neuron at –80 mV or 0 mV, respectively, during photostimulation of mPFC fibers.

(C) Traces of EPSCs evoked by stimulation of the AC-BLA pathway with or without priming photostimulation of mPFC fibers (red and black traces, respectively) with variable Δt (200–800 ms).

(D) PPR (50 ms interval) was increased in the AC-BLA pathway during heterosynaptic inhibition.

(E) EPSC amplitude inhibition as a function of Δt. mPFC priming induced significant inhibition of EPSCs with $\Delta t \leq 0.8$ s (n = 48 neurons).

(legend continued on next page)

et al., 2005) and that IL may project to the amygdala similarly to PL (Gutman et al., 2012; but see Vertes, 2004). The increased firing of mPFC neurons could potentially lead to exaggerated BLA activity during recall of extinction memory. The increases in BLA activity could, in fact, promote conditioned fear responses instead of suppressing them, as BLA sends direct excitatory projections to CeM output neurons (Paré et al., 1995; Pape and Pare, 2010). It is clear, however, that the BLA is a part of the extinction circuitry (Herry et al., 2008). How then could the enhanced activity of mPFC be translated into the suppressed fear response? Our results show that synaptic strength in projections from the mPFC to the BLA is decreased after fear extinction. This might serve as a compensatory plasticity mechanism, counterbalancing the increases in spiking frequency in the mPFC during recall of extinction memory. Our finding is in agreement with a previous study that reported that evoked field potentials in the BLA, induced by electrical stimulation of the mPFC in freely moving rats, were decreased after fear extinction (Vouimba and Maroun, 2011). Moreover, we found that GABA-mediated fast inhibitory synaptic responses remained unchanged in the mPFC-BLA pathway after fear extinction, resulting in reduced balance between monosynaptic glutamatergic EPSCs and disynaptic GABAergic IPSCs in this pathway. Thus, this mechanism may allow prevention of increased neuronal firing in the BLA during recall of extinction memory.

A majority of ITC neurons, positioned between the BLA and the CeA, were directly activated by mPFC in our experiments, exhibiting monosynaptic glutamatergic responses upon photostimulation of the corresponding fibers. This finding is in agreement with a previous study reporting that electrical stimulation of the IL/mPFC could result in reduced responsiveness of the CeM to inputs from the BLA (Quirk et al., 2003). As mPFC projections retained the ability to activate ITC neurons after extinction, increased neuronal firing in the mPFC during recall of extinction memory (Milad and Quirk, 2002; Holmes et al., 2012) would result in augmented inhibition of the CeM by ITC neurons through the mPFC-ITC-CeM pathway. Furthermore, activation of the mPFC-ITC projections could lead to depolarization of ITC neurons and may facilitate LTP induction in the BLA-ITC pathway implicated in fear extinction (Amano et al., 2010), resulting in further inhibition of the CeM and diminished fear responses.

Moreover, activation of local circuit interneurons in the BLA by mPFC fibers leads to heterosynaptic inhibition of synaptic transmission in convergent projections from the auditory cortex (AC) to the BLA (an auditory CS pathway). Heterosynaptic inhibition in the AC-BLA pathway, mediated by presynaptic $GABA_B$ receptors on AC terminals, is more pronounced at higher frequencies of mPFC activation. Therefore, it may diminish conditioned fear responses by suppressing the CS-evoked BLA activity during recall of extinction memory, which is associated with increased firing in mPFC neurons. Heterosynaptic inhibition might be more efficient in reducing the CS-evoked BLA activity than feedforward inhibition as it could be induced over longer periods of time (up to 800 ms after priming mPFC stimulation). This is because heterosynaptic inhibition is mediated by G protein-coupled $GABA_B$ receptors, whereas feedforward inhibition involves activation of ionotropic $GABA_A$ receptors with much faster kinetics of inactivation. Furthermore, the mPFC-mediated heterosynaptic inhibition in the AC-BLA pathway is enhanced after extinction training, thus providing an additional synaptic mechanism by which the expression of conditioned fear could be suppressed. Thus, encoding of fear extinction memory may implicate multiple mechanisms of both short- and long-term synaptic plasticity in the mPFC-amygdala circuits.

EXPERIMENTAL PROCEDURES

Stereotaxic Surgery and Viral Injections

Four-week-old male C57BL/6 mice (Charles River Laboratory) were used for stereotaxic viral injections. Small bilateral craniotomy was made targeting the infralimbic division of the medial prefrontal cortex (IL/mPFC) with stereotaxic coordinates (1.7 mm rostral to bregma, ±0.4 mm lateral to midline, and 2.6 mm ventral to bregma; Franklin and Paxinos, 2008). Glass capillaries with the tip size of 30 μm in outer diameter were loaded with high-titer adeno-associated virus (AAV) carrying CaMKIIα promoter and channelrhodopsin-2(H134R)-eYFP fusion gene (2–5 × 10^{12} viral particles/ml, serotype 5, packaged by the vector core facility at the University of North Carolina). Virus-containing solution was injected into both sides of the IL/mPFC (0.4–0.5 μl per side at a rate of 0.1 μl/min). All animal procedures in this study were approved by the Institutional Animal Care and Use Committee of McLean Hospital.

Behavioral Training

Mice were singly housed in home cages on a 12 hr light/dark cycle with food and water continuously available. Four weeks after surgery, mice were assigned to one of three groups: CS-only control, CS-US (fear conditioning), and fear extinction groups. Mice were handled for several days before behavioral training. On the training day (day 1), mice in the CS-only group were placed in the fear conditioning chamber (Med Associates) in context A and were given the CS (a 4 kHz pure tone lasting for 20 s) six times with a 2 min interval. Mice in the CS-US and fear extinction groups were given in context A six pairings of the CS and US, in which each CS was coterminated with the US (continuous foot shock for 2 s, 0.5 mA) with a 2 min interval

(F) PPR changes after mPFC priming (normalized to no priming control PPR). PPR was increased during mPFC priming-induced inhibition of EPSCs (n = 48 neurons).
(G) Correlation plot of the magnitude of heterosynaptic inhibition versus PPR changes (n = 48 neurons).
(H) Correlation plot of the magnitude of heterosynaptic inhibition versus peak amplitudes of priming IPSCs (n = 39 neurons).
(I) EPSCs in the AC-BLA pathway recorded 400 ms after priming stimulation of mPFC fibers (red traces) or without mPFC priming (black traces) in control external solution (left) or in the presence of CGP 52432 (10 μM, right).
(J) EPSC inhibition (%) in the AC-BLA pathway after mPFC priming under control conditions or in the presence of CGP 52432 (n = 6 neurons).
(K) PPR changes after mPFC priming with or without CGP 52432 in the external solution (n = 6 neurons).
(L) Heterosynaptic inhibition in the AC-BLA pathway with Δt = 400 ms in mice from CS-only, CS-US, and fear extinction groups. The intensity of priming photostimulation of the mPFC fibers was adjusted to generate EPSCs of the similar amplitudes in all three behavioral groups (no difference in the EPSC amplitudes between the groups, p = 0.91).
(M) Summary plots of heterosynaptic inhibition (n = 21, 18, and 19 cells from 6, 8, and 7 mice for CS-only, CS-US, and fear extinction groups, respectively).
(N) Same as in (M) but for PPR data. Error bars represent SEM.

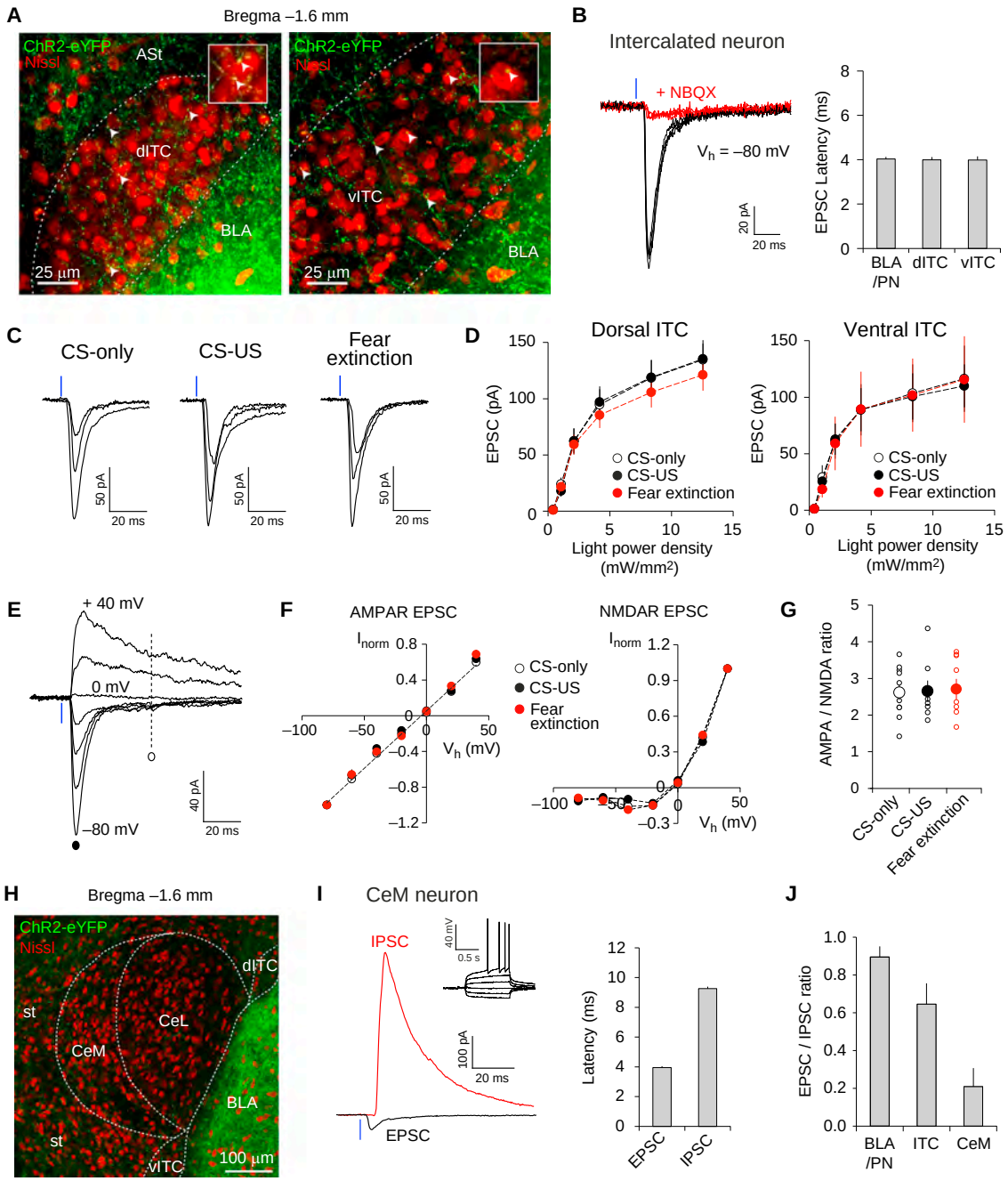

Figure 7. Direct Activation of Intercalated Neurons by Projections from the mPFC

(A) ChR2-eYFP-expressing mPFC fibers (green) in dorsolateral (dITC, left) and ventromedial (vITC, right) clusters of ITC neurons. Putative synaptic contacts are indicated as arrowheads. Ast, amygdalostriatal transition.

(B) Left: EPSCs in an intercalated neuron at –80 mV evoked by photostimulation of mPFC fibers. EPSCs were inhibited by NBQX (10 μM). Right: synaptic latencies of EPSCs in ITC neurons or BLA neurons (n = 21, 17, and 9 cells for BLA/PN, dITC, and vITC, respectively).

(C) EPSCs in the mPFC-ITC pathway in mice from each group induced by photostimuli of increasing intensity. EPSCs were recorded at –80 mV.

(D) Input-output curves of EPSCs in mPFC-dITC (left) and mPFC-vITC (right) pathways (mPFC-dITC: n = 20–33 cells from 7–10 mice per group; mPFC-vITC: n = 8–9 cells from 3–4 mice per group).

(E) EPSCs in the mPFC-ITC pathway at holding potentials from –80 to +40 mV in the presence of bicuculline (30 μM).

(F) I-V plots of EPSCs in the mPFC-ITC pathway. AMPAR- and NMDAR-mediated EPSCs were measured and normalized as in Figure 3D (data from both ITC clusters were pulled together; n = 8–11 cells from 5–7 mice per each group).

(G) AMPAR/NMDAR EPSC amplitude ratios in the mPFC-ITC pathway in different behavioral groups.

(legend continued on next page)

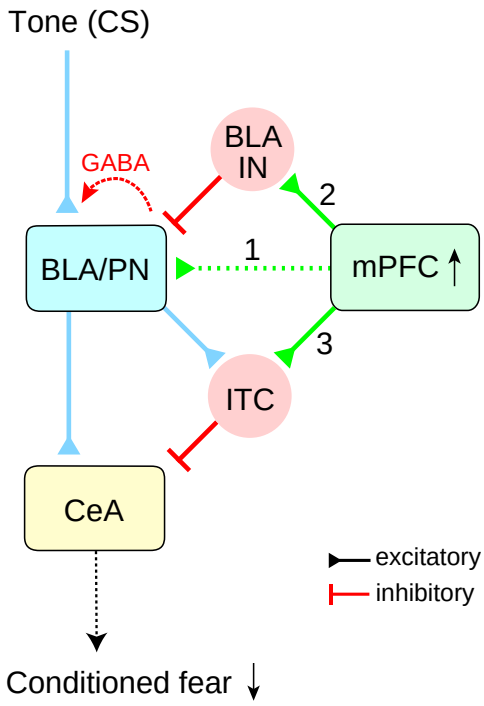

Figure 8. Modulatory Roles of the mPFC-Amygdala Pathways in Fear Extinction

After fear extinction, excitatory synaptic efficacy in the mPFC projections to principal neurons in the BLA (BLA/PN) decreases (1), resulting in a reduced balance between excitation and inhibition in this pathway. Projections from the mPFC also activate local GABAergic interneurons (BLA/IN; 2), which, in turn, induce heterosynaptic inhibition of the AC-BLA pathway, an auditory CS input. Synaptic efficacy in direct mPFC inputs to intercalated (ITC) neurons remains unchanged after extinction training (3). Therefore, increased activity of the mPFC during recall of extinction memory (Milad and Quirk, 2002; Holmes et al., 2012) would induce more efficient heterosynaptic inhibition in the AC-BLA pathway and more frequent activation of ITC neurons, resulting in robust inhibitory responses in the CeA (specifically, CeM), the output nucleus of the amygdala. Through these mechanisms, the mPFC could attenuate the spiking output of the amygdala during the CS presentation, thus suppressing the conditioned fear response after fear extinction.

between CS-US pairings. On day 2, mice in the CS-only and CS-US groups were left in a home cage, whereas mice in the extinction group were placed in the fear conditioning chamber in context B and presented with 20 CS with a 50 s interval between CS presentations. On the test day (day 3), mice in all three groups were placed in the fear conditioning chamber in context B. After a 1–2 min habituation period, freezing responses to two CS presentations with a 50 s interval were measured. Fear conditioning, extinction training, and freeze testing was performed between 10 and 11 a.m. The room temperature was 22°C–23°C. The movement of mice in the fear conditioning chamber was video recorded using a near infrared camera and analyzed with Videofreeze software (Med Associates). Freezing score was calculated as the percentage of time of the total CS duration when mice remained immobile (frozen). The bout length was 2 s. Different tactile (stainless steel grid or acrylic floor), visual (with or without white house light), and olfactory cues (0.25% benzaldehyde or 2% acetic acid) were used for different contexts (context A versus context B).

Electrophysiology

After testing freezing responses to the CS, mice were anesthetized with a mixture of ketamine and xylazine (160 mg/kg and 12 mg/kg body weight, respectively, intramuscular injection) and decapitated. Brains were dissected quickly and chilled in ice-cold artificial cerebrospinal fluid (ACSF) containing 130 mM NaCl, 2.5 mM KCl, 2.5 mM $CaCl_2$, 1 mM $MgSO_4$, 1.25 mM NaH_2PO_4, 26 mM $NaHCO_3$, and 10 mM glucose with 95% O_2 and 5% CO_2. Coronal brain slices containing either the mPFC or the amygdala (300 μm thick) were prepared with a vibratome. After recovery, slices were placed in the recording chamber and continuously perfused with the ACSF at the rate of ~1 ml per minute. For most whole-cell recordings, the patch electrodes (2–3 MΩ resistance) were filled with Cs^+-based pipette solution with low $[Cl^-]_{in}$ (12 mM) containing 140 mM Cs-methanesulfonate, 5 mM NaCl, 1 mM $MgCl_2$, 10 mM HEPES, 0.2 EGTA, 2 mM MgATP, 0.5 mM NaGTP, 0.5 mM spermine, and 5 mM QX 314 chloride (290 mOsm, adjusted to pH 7.3 with CsOH). In recordings from interneurons in the BLA (Figures 4B, 4C, 5A–5G, S3F, S7C, and S7G), 140 mM Cs-methanesulfonate was replaced with 150 mM K-gluconate without QX 314 or spermine added. This K^+-based pipette solution was also used for recordings from BLA principal neurons in Figures 1C, 2E–2F, 3F–3J, and S7F. In some recordings of IPSCs in principal neurons in the BLA (Figures 5H–5N and S7H–S7J), we used Cs^+-based pipette solution with high $[Cl^-]_{in}$ (132 mM) containing 120 mM CsCl, 20 mM Cs-methanesulfonate, 5 mM NaCl, 1 mM MgCl2, 10 mM HEPES, 0.2 EGTA, 2 mM MgATP, 0.5 mM NaGTP, 0.5 mM spermine, and 5 mM QX 314 chloride. Whole-cell patch-clamp recordings were performed at 30°C–31°C using EPC-9 amplifier and Pulse v8.8 software (HEKA Elektronik). Membrane potential was held constant at –80 mV in a voltage-clamp mode unless indicated otherwise. Liquid junction potential of 8.9 mV, 4.1 mV, and 15.5 mV was corrected for the Cs-based pipette solution with low and high $[Cl^-]_{in}$ and for K-gluconate-based pipette solution, respectively. Series (access) resistance was <15 MΩ, and it was not compensated. Offline data analysis was performed using Clampfit 9 program (Molecular Devices).

Photostimulation

Blue collimated light-emitting diode (LED) with 470 nm peak wavelength (M470L2, Thorlabs) was used for photostimulation of ChR2-expressing mPFC fibers. The LED was connected to EPC-9 amplifier or Master-8 Pulse Stimulator through the LED driver (LEDD1B, Thorlabs). Brain slices in recording chamber were illuminated through 40× water-immersion objective lens (IR-Achroplan, Carl Zeiss) and a fluorescent pathway with excitation (470 nm) and emission (505–530 nm) filters (filter set 13, Carl Zeiss). Illumination area was 0.26 mm^2 and was centered at the soma of the neuron patched for recording. To evoke synaptic responses in the amygdala by photostimulation of mPFC fibers, we illuminated slices every 10 s with blue light pulses of a short duration (1–3 ms for neurons in LA and BLA and 3–5 ms for intercalated neurons and neurons in the CeA). In experiments in Figures 2J–2L, 5-ms-long photostimulation pulses were used. In experiments in Figures S3A–S3G, 10-ms-long photostimulation were used.

Histology and Microscopy

After electrophysiological recordings, slices were fixed in 4% paraformaldehyde-containing PBS at 4°C overnight. After fixation, slices were incubated with Neurotrace Fluoresent Nissl stain (diluted 40-fold in PBS, 615 nm emission wavelength, Molecular Probes). Images for Nissl stain (red fluorescence)

(H) Sparse innervation of the CeA by ChR2-eYFP-expressing mPFC fibers (green). CeL and CeM, lateral and medial divisions of the CeA, respectively. st, the stria terminalis.
(I) Left: EPSC (black) and IPSC (red) recorded in a CeM neuron in voltage-clamp mode at –80 mV and 0 mV, respectively. Inset: spiking response of a CeM neuron to depolarizing current injection. Right: IPSCs had longer latencies compared to EPSCs (n = 13 and 30 neurons for EPSCs and IPSCs, respectively; $p < 0.0001$).
(J) A summary plot of EPSC/IPSC ratios in BLA/PN, ITC neurons and CeM neurons (n = 21, 9, and 28 cells for BLA/PN, ITC neurons, and CeM neurons, respectively). Error bars represent SEM.

and ChR2-eYFP (green fluorescence) were captured using Leica TCS SP8 Confocal System (Leica) or Axioskop 2 fluorescent microscope (Carl Zeiss). For each mouse, a virus injection site was verified by identifying ChR2-eYFP expression in the mPFC. Mice in which the target area was missed were excluded from the analysis.

Data Analysis

Data are presented as means ± SEM. For statistical comparisons, we used Student's t test or ANOVA with Bonferroni's simultaneous multiple comparisons unless indicated otherwise (see Tables S1 and S2 for details). Statistical analysis was performed with Minitab16 software (Minitab), and $p < 0.05$ was considered statistically significant.

Additional Methods

An extended version of the experimental procedures is available online in the Supplemental Experimental Procedures.

SUPPLEMENTAL INFORMATION

Supplemental Information includes Supplemental Experimental Procedures, eight figures, and two tables and can be found with this article online at http://dx.doi.org/10.1016/j.neuron.2013.09.025.

ACKNOWLEDGMENTS

We thank Yan Li for constructive discussions and Elif Engin, Alexei Morozov and Wataru Ito for experimental advices. This study was supported by Whitehall Foundation (V.Y.B.) and NIH grants MH083011 and MH090464 (V.Y.B.).

Accepted: September 13, 2013
Published: November 27, 2013

REFERENCES

Amano, T., Unal, C.T., and Paré, D. (2010). Synaptic correlates of fear extinction in the amygdala. Nat. Neurosci. *13*, 489–494.

Amir, A., Amano, T., and Pare, D. (2011). Physiological identification and infralimbic responsiveness of rat intercalated amygdala neurons. J. Neurophysiol. *105*, 3054–3066.

Boyden, E.S., Zhang, F., Bamberg, E., Nagel, G., and Deisseroth, K. (2005). Millisecond-timescale, genetically targeted optical control of neural activity. Nat. Neurosci. *8*, 1263–1268.

Burgos-Robles, A., Vidal-Gonzalez, I., and Quirk, G.J. (2009). Sustained conditioned responses in prelimbic prefrontal neurons are correlated with fear expression and extinction failure. J. Neurosci. *29*, 8474–8482.

Cho, J.H., Bayazitov, I.T., Meloni, E.G., Myers, K.M., Carlezon, W.A., Jr., Zakharenko, S.S., and Bolshakov, V.Y. (2012). Coactivation of thalamic and cortical pathways induces input timing-dependent plasticity in amygdala. Nat. Neurosci. *15*, 113–122.

Franklin, K.B.J., and Paxinos, G. (2008). The Mouse Brain in Stereotaxic Coordinates. (San Diego: Academic Press).

Gabbott, P.L., Warner, T.A., Jays, P.R., Salway, P., and Busby, S.J. (2005). Prefrontal cortex in the rat: projections to subcortical autonomic, motor, and limbic centers. J. Comp. Neurol. *492*, 145–177.

Gutman, D.A., Keifer, O.P., Jr., Magnuson, M.E., Choi, D.C., Majeed, W., Keilholz, S., and Ressler, K.J. (2012). A DTI tractography analysis of infralimbic and prelimbic connectivity in the mouse using high-throughput MRI. Neuroimage *63*, 800–811.

Herry, C., and Garcia, R. (2002). Prefrontal cortex long-term potentiation, but not long-term depression, is associated with the maintenance of extinction of learned fear in mice. J. Neurosci. *22*, 577–583.

Herry, C., Ciocchi, S., Senn, V., Demmou, L., Müller, C., and Lüthi, A. (2008). Switching on and off fear by distinct neuronal circuits. Nature *454*, 600–606.

Holmes, A., Fitzgerald, P.J., MacPherson, K.P., DeBrouse, L., Colacicco, G., Flynn, S.M., Masneuf, S., Pleil, K.E., Li, C., Marcinkiewcz, C.A., et al. (2012). Chronic alcohol remodels prefrontal neurons and disrupts NMDAR-mediated fear extinction encoding. Nat. Neurosci. *15*, 1359–1361.

Katz, L.C., Burkhalter, A., and Dreyer, W.J. (1984). Fluorescent latex microspheres as a retrograde neuronal marker for in vivo and in vitro studies of visual cortex. Nature *310*, 498–500.

LeDoux, J.E. (2000). Emotion circuits in the brain. Annu. Rev. Neurosci. *23*, 155–184.

Likhtik, E., Popa, D., Apergis-Schoute, J., Fidacaro, G.A., and Paré, D. (2008). Amygdala intercalated neurons are required for expression of fear extinction. Nature *454*, 642–645.

Maren, S., and Quirk, G.J. (2004). Neuronal signalling of fear memory. Nat. Rev. Neurosci. *5*, 844–852.

McKernan, M.G., and Shinnick-Gallagher, P. (1997). Fear conditioning induces a lasting potentiation of synaptic currents in vitro. Nature *390*, 607–611.

Milad, M.R., and Quirk, G.J. (2002). Neurons in medial prefrontal cortex signal memory for fear extinction. Nature *420*, 70–74.

Milad, M.R., Vidal-Gonzalez, I., and Quirk, G.J. (2004). Electrical stimulation of medial prefrontal cortex reduces conditioned fear in a temporally specific manner. Behav. Neurosci. *118*, 389–394.

Myers, K.M., and Davis, M. (2007). Mechanisms of fear extinction. Mol. Psychiatry *12*, 120–150.

Pape, H.C., and Pare, D. (2010). Plastic synaptic networks of the amygdala for the acquisition, expression, and extinction of conditioned fear. Physiol. Rev. *90*, 419–463.

Paré, D., Smith, Y., and Paré, J.F. (1995). Intra-amygdaloid projections of the basolateral and basomedial nuclei in the cat: Phaseolus vulgaris-leucoagglutinin anterograde tracing at the light and electron microscopic level. Neuroscience *69*, 567–583.

Pavlov, I.P. (1927). Conditioned Reflexes: An Investigation of the Physiological Activity of the Cerebral Cortex. (London: Oxford University Press).

Petreanu, L., Mao, T., Sternson, S.M., and Svoboda, K. (2009). The subcellular organization of neocortical excitatory connections. Nature *457*, 1142–1145.

Quirk, G.J., Repa, C., and LeDoux, J.E. (1995). Fear conditioning enhances short-latency auditory responses of lateral amygdala neurons: parallel recordings in the freely behaving rat. Neuron *15*, 1029–1039.

Quirk, G.J., Russo, G.K., Barron, J.L., and Lebron, K. (2000). The role of ventromedial prefrontal cortex in the recovery of extinguished fear. J. Neurosci. *20*, 6225–6231.

Quirk, G.J., Likhtik, E., Pelletier, J.G., and Paré, D. (2003). Stimulation of medial prefrontal cortex decreases the responsiveness of central amygdala output neurons. J. Neurosci. *23*, 8800–8807.

Rogan, M.T., Stäubli, U.V., and LeDoux, J.E. (1997). Fear conditioning induces associative long-term potentiation in the amygdala. Nature *390*, 604–607.

Royer, S., Martina, M., and Paré, D. (1999). An inhibitory interface gates impulse traffic between the input and output stations of the amygdala. J. Neurosci. *19*, 10575–10583.

Santini, E., Ge, H., Ren, K., Peña de Ortiz, S., and Quirk, G.J. (2004). Consolidation of fear extinction requires protein synthesis in the medial prefrontal cortex. J. Neurosci. *24*, 5704–5710.

Santini, E., Quirk, G.J., and Porter, J.T. (2008). Fear conditioning and extinction differentially modify the intrinsic excitability of infralimbic neurons. J. Neurosci. *28*, 4028–4036.

Shaban, H., Humeau, Y., Herry, C., Cassasus, G., Shigemoto, R., Ciocchi, S., Barbieri, S., van der Putten, H., Kaupmann, K., Bettler, B., and Lüthi, A. (2006). Generalization of amygdala LTP and conditioned fear in the absence of presynaptic inhibition. Nat. Neurosci. *9*, 1028–1035.

Shin, R.M., Tsvetkov, E., and Bolshakov, V.Y. (2006). Spatiotemporal asymmetry of associative synaptic plasticity in fear conditioning pathways. Neuron *52*, 883–896.

Takagishi, M., and Chiba, T. (1991). Efferent projections of the infralimbic (area 25) region of the medial prefrontal cortex in the rat: an anterograde tracer PHA-L study. Brain Res. *566*, 26–39.

Tsvetkov, E., Carlezon, W.A., Benes, F.M., Kandel, E.R., and Bolshakov, V.Y. (2002). Fear conditioning occludes LTP-induced presynaptic enhancement of synaptic transmission in the cortical pathway to the lateral amygdala. Neuron *34*, 289–300.

Vertes, R.P. (2004). Differential projections of the infralimbic and prelimbic cortex in the rat. Synapse *51*, 32–58.

Vouimba, R.M., and Maroun, M. (2011). Learning-induced changes in mPFC-BLA connections after fear conditioning, extinction, and reinstatement of fear. Neuropsychopharmacology *36*, 2276–2285.

Zucker, R.S., and Regehr, W.G. (2002). Short-term synaptic plasticity. Annu. Rev. Physiol. *64*, 355–405.